applied sciences

MDPI

Article

A Quantitative Investigation on the Peripheral Nerve Response within the Small Strain Range

Elisabetta Giannessi [1,†], Maria Rita Stornelli [1], Alessandra Coli [1] and Pier Nicola Sergi [2,*,†]

[1] Department of Veterinary Science, University of Pisa, 56124 Pisa, Italy; elisabetta.giannessi@unipi.it (E.G.); maria.rita.stornelli@unipi.it (M.R.S.); alessandra.coli@unipi.it (A.C.)

[2] Computational Neuroengineering Lab, Translational Neural Engineering Area, The Biorobotics Institute, Sant'Anna School of Advanced Studies, PSV, 56025 Pontedera, Italy

* Correspondence: p.sergi@sssup.it

† These authors contributed equally to this work.

Received: 15 February 2019; Accepted: 12 March 2019; Published: 16 March 2019

Abstract: Peripheral nerves are very complex biological structures crucial to linking the central nervous system to the periphery of the body. However, their real behaviour is partially unknown because of the intrinsic difficulty of studying these structures in vivo. As a consequence, theoretical and computational tools together with in vitro experiments are widely used to approximate the mechanical response of the peripheral nervous tissue to different kind of solicitations. More specifically, particular conditions narrow the mechanical response of peripheral nerves within the small strain regime. Therefore, in this work, the mechanical response of nerves was investigated through the study of the relationships among strain, stress and displacements within the small strain range. Theoretical predictions were quantitatively compared to experimental evidences, while the displacement field was studied for different values of the tissue compressibility. This framework provided a straightforward computational assessment of the nerve response, which was needed to design suitable connections to biomaterials or neural interfaces within the small strain range.

Keywords: peripheral nerves biomechanics; computational neuromechanics; computational neuroscience; small strain range

1. Introduction

Peripheral nerves are composed by several cellular elements, as Schwann cells, perineurial cells, and axons (neuronal processes), enveloped by connective tissue [1]. The axons could be originated from centrally or peripheral neurons, while the Schwann cell coats, which envelop axons, are placed within a circumferential layer of perineurial cells. Similarly, the perineurial coat lies within epineurium, which is a soft tissue rich in fibroblasts, collagen fibers, and small blood vessels [2]. Since peripheral nerves have unique anatomical characteristics, due to the very high ratio between their cross sectional area and their distance with respect to the parent cell body [3], they have extrinsic and intrinsic blood supply [4,5]. More specifically, nutritive arteries, arterioles, and venules, which run with the epineural vessels, belong to the extrinsic system, while longitudinal microvessels within the endoneural space belong to the intrinsic system [3].

Depolarization potentials travel through neurons packed within nerves, then peripheral nerves link the central nervous system to the periphery of the body. Afferent nerves, link muscles and external sensory receptors to the CNS, while in efferent nerves the information travel in the other direction. Peripheral nerves could be classified as motor nerves, which target muscles, sensory nerves, which target sensory receptors and mixed nerves, in which both motor and sensory fibers are packed together [1,3,6].

Anatomical investigations of peripheral nerves were extensively performed [6,7] and sometimes they were related to biomechanical considerations [8,9]. In particular, tissue mechanics was used in combination with finite element analysis [10–12] to explore the behaviour of nerves in presence of different stimuli [13–16]. Indeed, a quantitative assessment of the nerve response could be interesting for several applications, as neuroprosthetics [17,18], neural interfaces design [19,20] and interaction with biomedical devices (e.g., microneedles [21–23]).

In particular conditions, peripheral nerves are elongated only of a small extent, as in case of movements constrained after medical interventions (e.g., immobilization procedures), or in case of neuropathic tremors [24], or for voluntary/involuntary small and quick movements involving articulations [25]. Therefore, this kind of response could be interesting "per se", as well as to evaluate the coupling between nerves and biomaterials, as for acute or chronic implantation of medical devices, interacting with the nervous tissue in these conditions [17]. Nevertheless, the nerve behaviour within the small strain range is a less investigated topic, while the response to higher strains was explored in some greater details [13–16,25]. In particular, the displacement field arising within the small strain regime (i.e., $0 < \epsilon << 0.1$) was theoretically predicted together with the effects of the variation of the tissue compressibility on the nerve response. In addition, numerical results were quantitatively compared to experimental data to test the suitability of the presented framework.

2. Materials and Methods

2.1. Theoretical Framework

To investigate the behaviour of the peripheral nerves within the small strain range, the nervous tissue was modelled as a solid material, for which the general equilibrium equations [26] in every point of the volume were:

$$\frac{\partial \sigma_{xx}}{\partial x} + \frac{\partial \sigma_{yx}}{\partial y} + \frac{\partial \sigma_{zx}}{\partial z} + X = 0 \tag{1}$$

$$\frac{\partial \sigma_{xy}}{\partial x} + \frac{\partial \sigma_{yy}}{\partial y} + \frac{\partial \sigma_{zy}}{\partial z} + Y = 0 \tag{2}$$

$$\frac{\partial \sigma_{xz}}{\partial x} + \frac{\partial \sigma_{yz}}{\partial y} + \frac{\partial \sigma_{zz}}{\partial z} + Z = 0 \tag{3}$$

where σ_{ij} were the components of the stress tensor ($i, j = x, y, z$) and X, Y, Z were body forces. Moreover, for the lateral surface of the solid the boundary conditions were:

$$\sigma_{xx}\alpha_x + \sigma_{yx}\alpha_y + \sigma_{zx}\alpha_z = p_x \tag{4}$$

$$\sigma_{xy}\alpha_x + \sigma_{yy}\alpha_y + \sigma_{zy}\alpha_z = p_y \tag{5}$$

$$\sigma_{xz}\alpha_x + \sigma_{yz}\alpha_y + \sigma_{zz}\alpha_z = p_z \tag{6}$$

where p_x, p_y, p_z were the external pressure acting on the lateral surface and $\alpha_x, \alpha_y, \alpha_z$ were the directions of action for each pressure. The peripheral nervous tissue was assumed as a linear elastic body, which in addition was homogeneous and isotropic. As a consequence, the following relationships between components of deformation and tension hold:

$$E\epsilon_{xx} = \sigma_{xx} - \nu(\sigma_{yy} + \sigma_{zz}) \tag{7}$$

$$E\epsilon_{yy} = \sigma_{yy} - \nu(\sigma_{xx} + \sigma_{zz}) \tag{8}$$

$$E\epsilon_{zz} = \sigma_{zz} - \nu(\sigma_{yy} + \sigma_{xx}) \tag{9}$$

$$G\epsilon_{xy} = \sigma_{xy} \tag{10}$$

$$G\epsilon_{xz} = \sigma_{xz} \tag{11}$$

$$G\epsilon_{yz} = \sigma_{yz} \tag{12}$$

where E was the Young modulus, ν was the Poisson coefficient, and $G = \frac{E}{2(1+\nu)}$ was the shear modulus. More specifically, in our case, the body forces were assumed to be negligible with respect to the other applied forces, then $X, Y, Z = 0$. Similarly, $\alpha_z = 0$ and $p_x, p_y, p_z = 0$, thus Equations (1)–(3) became:

$$\frac{\partial \sigma_{xx}}{\partial x} + \frac{\partial \sigma_{yx}}{\partial y} + \frac{\partial \sigma_{zx}}{\partial z} = 0 \tag{13}$$

$$\frac{\partial \sigma_{xy}}{\partial x} + \frac{\partial \sigma_{yy}}{\partial y} + \frac{\partial \sigma_{zy}}{\partial z} = 0 \tag{14}$$

$$\frac{\partial \sigma_{xz}}{\partial x} + \frac{\partial \sigma_{yz}}{\partial y} + \frac{\partial \sigma_{zz}}{\partial z} = 0 \tag{15}$$

while Equations (4)–(6) became:

$$\sigma_{xx}\alpha_x + \sigma_{yx}\alpha_y = 0 \tag{16}$$

$$\sigma_{xy}\alpha_x + \sigma_{yy}\alpha_y = 0 \tag{17}$$

$$\sigma_{xz}\alpha_x + \sigma_{yz}\alpha_y = 0 \tag{18}$$

A tensional state compatible with the physiological loading conditions of the nerve was $\sigma_{xx} = \sigma_{yy} = 0, \sigma_{zz} \in R$. Therefore, Equations (7)–(12), gave the components of the deformation tensor. Equations (13)–(15), which gave the tensional state within the nerve volume, were satisfied, as well as Equations (16)–(18), which provided the boundary conditions on the lateral surface of the specimen. The resulting deformation tensor was written as:

$$\mathbf{e} = \frac{\sigma_{zz}}{E}\left[-\nu \mathbf{i} \otimes \mathbf{i} - \nu \mathbf{j} \otimes \mathbf{j} + \mathbf{k} \otimes \mathbf{k}\right] \tag{19}$$

where **i**,**j**,**k** were the unit vectors along the x, y, z axes. The components of displacement field were, then, derived from the integral functions:

$$u(x) = \int_0^x \epsilon_{xx}(\xi) d\xi \tag{20}$$

$$v(y) = \int_0^y \epsilon_{yy}(\eta) d\eta \tag{21}$$

$$w(z) = \int_0^z \epsilon_{zz}(\theta) d\theta \tag{22}$$

Finally, the displacement in a point of the volume was written in vectorial form as:

$$\mathbf{d}(x, y, z) = u(x)\mathbf{i} + v(y)\mathbf{j} + w(z)\mathbf{k} \tag{23}$$

while the amount of displacement was given by $|\mathbf{d}(x, y, z)|$. The nervous tissue was considered almost fully incompressible. As a consequence, the value of the Poisson ratio was provided by the incompressibility constraint, which lead to:

$$\nu = lim_{\epsilon_{zz} \to 0} \frac{1}{\epsilon_{zz}} \left(1 - \frac{1}{\sqrt{1 + \epsilon_{zz}}}\right) \tag{24}$$

This limit value was calculated through the De l'Hospital theorem, which provided $lim_{\epsilon_{zz} \to 0} \nu = \frac{1}{2}$. However, the general form of the complementary potential [26] for the linear elastic material was:

$$\Psi = \frac{A}{2E} - \frac{\nu B}{E} + \frac{C}{2G} \tag{25}$$

where $A = \sigma_{xx}^2 + \sigma_{yy}^2 + \sigma_{zz}^2$, $B = \sigma_{xx}\sigma_{yy} + \sigma_{xx}\sigma_{zz} + \sigma_{yy}\sigma_{zz}$, $C = \sigma_{xy}^2 + \sigma_{xz}^2 + \sigma_{yz}^2$. Equation (25) was positive defined for tensions different from 0 only if the Hessian was positive together with all its principal minors, thus this condition lead to $E > 0$ and $-1 < \nu < \frac{1}{2}$. As a consequence the value of the Poisson ration was written as:

$$\nu(\omega) = \frac{1}{2+\omega} \tag{26}$$

where $\omega \in R^+$ and $\omega \to 0$ to account for this further constraint. Similarly, the bulk and the shear moduli were computed as:

$$K(E, \omega) = \frac{E(2+\omega)}{3\omega} \tag{27}$$

and

$$G(E, \omega) = \frac{E(2+\omega)}{2(3+\omega)} \tag{28}$$

Therefore, Equations (20)–(22) accounting for Equation (26) and making explicit all dependencies resulted in

$$u(x, E, \omega, \sigma_{zz}) = \frac{-\sigma_{zz}}{E(2+\omega)}x + u_0(x) \tag{29}$$

$$v(y, E, \omega, \sigma_{zz}) = \frac{-\sigma_{zz}}{E(2+\omega)}y + v_0(y) \tag{30}$$

$$w(z, E, \sigma_{zz}) = \frac{\sigma_{zz}}{E}z + w_0(z) \tag{31}$$

where $u_0(x), v_0(y), w_0(z)$, were functions due to a rigid motion, which, for sake of simplicity, were set to zero.

2.2. Stretching Experiments

A specimen was taken from a sciatic nerve, previously dissected from a posterior limb of a Large White pig (∼10 months old, slaughtered in conformity with the Italian National Regulation and frozen until experiments). Before experiments, the nerve specimen (65 mm long with a cross-sectional area of ∼11.18 mm^2) was gradually defrosted and re-hydrated for about one hour at room temperature in a bath of aqueous saline solution isotonic to the blood (0.9% sodium chloride) to minimize the time dependence of the tissue hydration. Experiments were then performed at room temparature (∼25 ± 1 °C) through an Instron R4464 testing machine (Instron Corporation, Canton, MA, USA) and with a standard load cell (Instron load cell, Instron Corporation, cell type 2525-808, max force 10 N, accuracy 0.25% Full Scale Output). The length of the specimen between clamps was 55 mm, and its physiological characteristics were kept by regularly spraying saline moisture on its external surface, in order to maintain the initial level of hydration. More specifically, the nerve was stretched (velocity $v = 10$ mm/min [27]; maximum strain 5%) after preconditioning to minimize viscoelastic effects [28]. The axial force was digitally recorded for five extensions of the nerve.

3. Results

Experimental data were shown (white circles) for five consecutive extensions together with the theoretical prediction coming from Equation (19), which was plotted through a bold line (Figure 1a). The range of variation of the Cauchy stress was between 0 (reference configuration) and 1.183 kPa when the strain ranged between $\epsilon = 0$ and $\epsilon = 0.05$. In this range the predicted stiffness was $E = 21.188$ kPa, and the axial component of Equation (19) was able to closely reproduce the experimental evolution of stress ($R^2 = 0.997$). The distribution of errors, which were accounted for as the difference

between experimental data and the theoretical prediction of the mean Cauchy stress, was shown in Figure 1b. The distribution of errors had a peak of probability (around 8.5%) for values ranging between −0.020 kPa and −0.015 kPa, while the maximum error was 0.104 kPa (around 0.5%), which represented a deviation from linearity of about 8.8%.

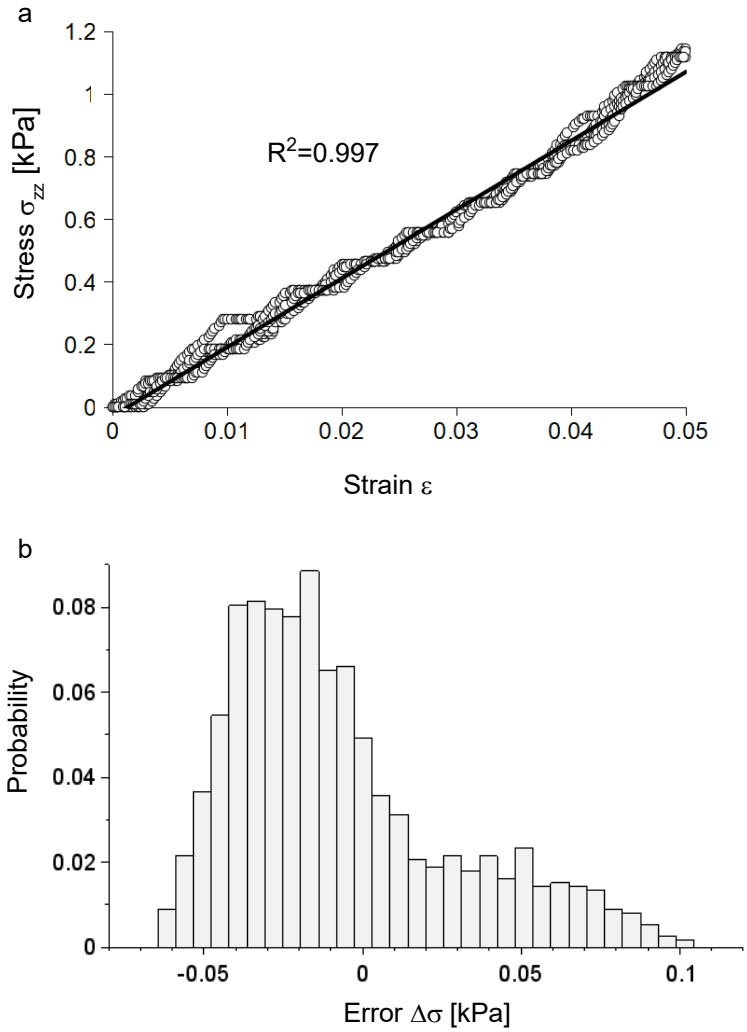

Figure 1. (**a**) Experimental data for five consecutive extensions together with the theoretical prediction (bold line), which was able to closely reproduce the experimental evolution of stress ($R^2 = 0.997$). (**b**) The distribution of errors had a peak of probability (around 8.5%) for values ranging between −0.020 kPa and −0.015 kPa, while the maximum error was 0.104 kPa (around 0.5%), which represented a deviation from linearity of about 8.8%.

The theoretical evolution of the axial displacement was studied for a fully incompressible nervous specimen with a length of 55 mm and cross sectional eccentricity of 0.95. Therefore, the transversal area was approximated with a "tape like" structure (1.398 mm × 4.000 mm). The axial field of displacements was linearly increasing with the z coordinate, thus the boundary conditions to the limit sections, (i.e., $z = 0$, $z = 55$ mm) were automatically satisfied. Since the solution was expressed only as a function of the z coordinate, it was invariant with respect to × and y, and the displacement field had the form displayed in Figure 2a. The lateral contraction was also investigated and, for each axis (x and y), the displacement field was expressed as a function of only one variable (respectively x and y). In both cases, the field of displacements was symmetric with respect to the central axis, as well as invariant with respect to the z coordinate, as shown in Figure 2b,c.

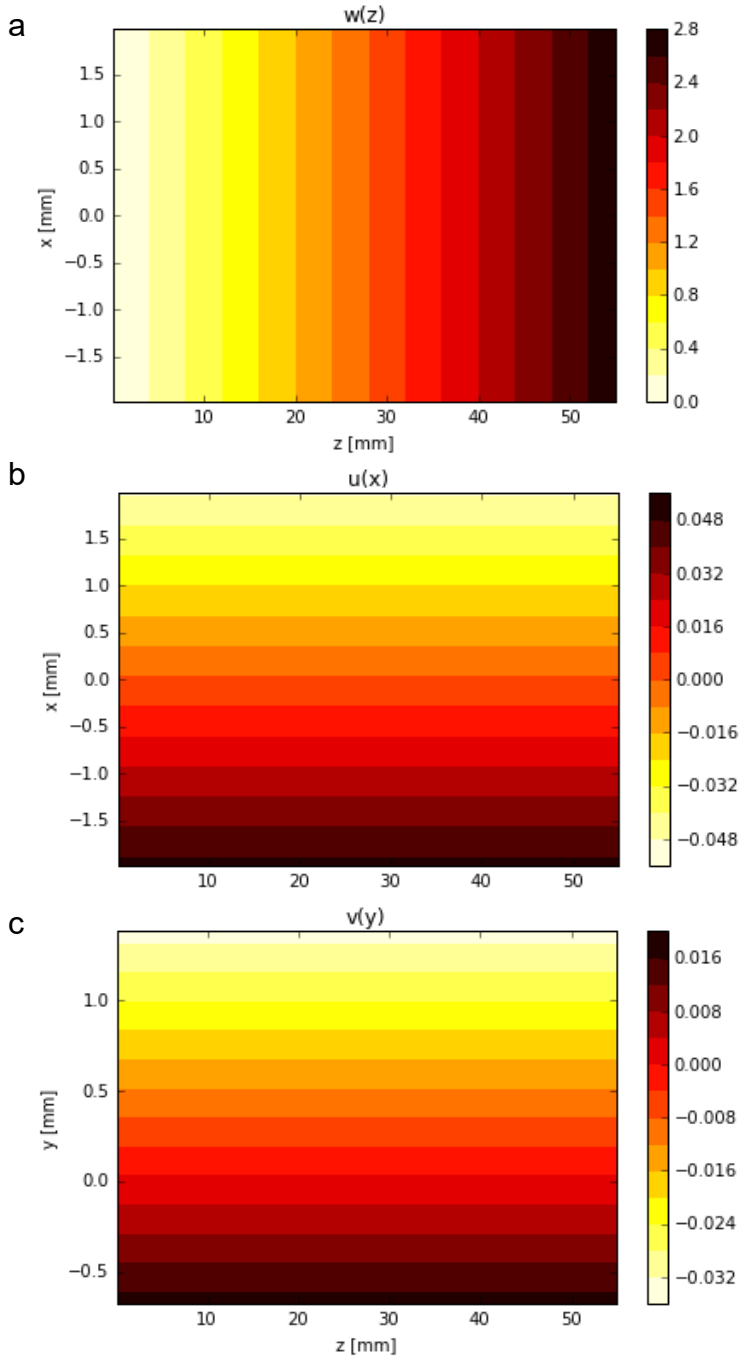

Figure 2. (**a**) The theoretical evolution of the axial displacement for a fully incompressible nervous specimen with a length of 55 mm and a section of 1.398 mm × 4.000 mm; the axial field of displacements was linearly increasing with the z coordinate. (**b**) Lateral contraction; the displacement field was expressed as a function of x. (**c**) Lateral contraction: the displacement field was expressed as a function of y. In both cases, the field of displacements was symmetric with respect to the central axis as well as invariant with respect to the z coordinates.

Moreover, the compressibility of the material was varied and, in Figure 3a, the evolution of the Poisson ratio was shown for increasing values of the ω parameter. In particular, the Poisson ratio assumed the values of $\nu \simeq 0.499$ for $\omega = 1 \times 10^{-12}$, $\nu \simeq 0.476$, for $\omega = 0.1$ and $\nu = 0.334$ for $\omega = 1$. Similarly, the variation of the bulk modulus, which was related to the compressibility parameter ω through Equation (27), was shown in Figure 3b. For $E = 21.188$ kPa, together with the previous values of compressibility, the bulk modulus assumed the following values 1.413×10^{13}, 148.316, 21.188 kPa.

In a similar way, the evolution of the shear modulus, related to ω through Equation (28), was shown in Figure 3c. In this case, the shear modulus values for $\omega = 1 \times 10^{-12}, 0.1.1$ were respectively $G = 7.063, 7.177, 7.945$ kPa.

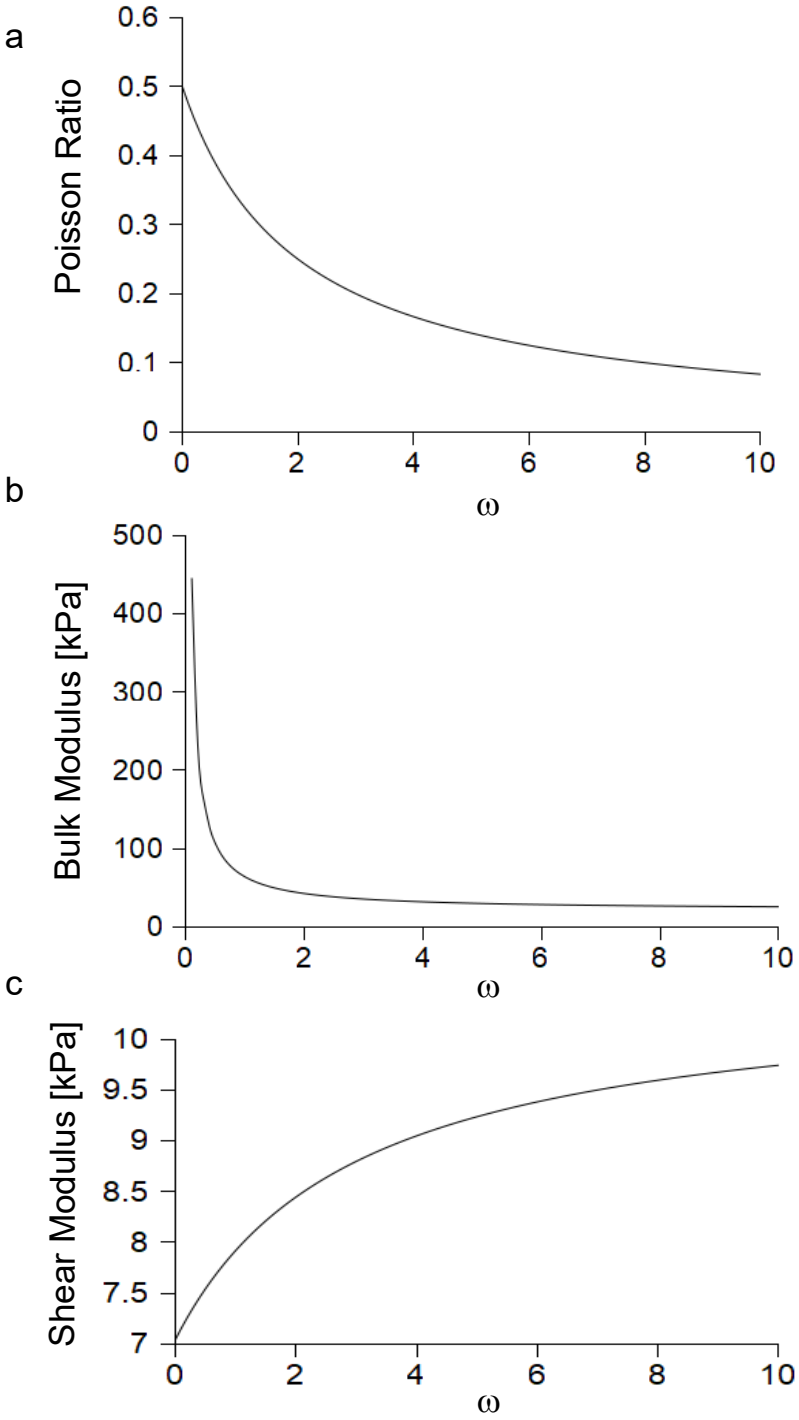

Figure 3. (**a**) Evolution of the Poisson ratio with the variation of the compressibility parameter ω. (**b**) Evolution of the bulk modulus with the variation of the compressibility parameter ω. (**c**) Evolution of the shear modulus with the variation of the compressibility parameter ω.

The effect of the variation of compressibility was studied on the lateral contraction of the strained nerve. First, in Figure 4a, the evolution of the amount of contraction was studied for $\epsilon = 0.05$ (i.e., maximum strain) for different and symmetric distances from the neutral line (which was, in all cases, a

symmetry axis) and for variations of the compressibility parameter (i.e, $0 < \omega \leq 2$). Then, the evolution of the lateral contraction with the variation of the distance from the center of the nerve section was shown in Figure 4b for $0 \leq \epsilon \leq 0.05$ and for a very low value of the compressibility parameter $\omega = 1 \times 10^{-12}$ (i.e., fully incompressible solid). Similarly, the evolution of the lateral contraction with the variation of the distance from the center of the nerve section was shown in Figure 4c for both a nearly incompressible and a compressible solid (respectively $\omega = 0.1$ and $\omega = 1$) for a strain range of $0 \leq \epsilon \leq 0.05$.

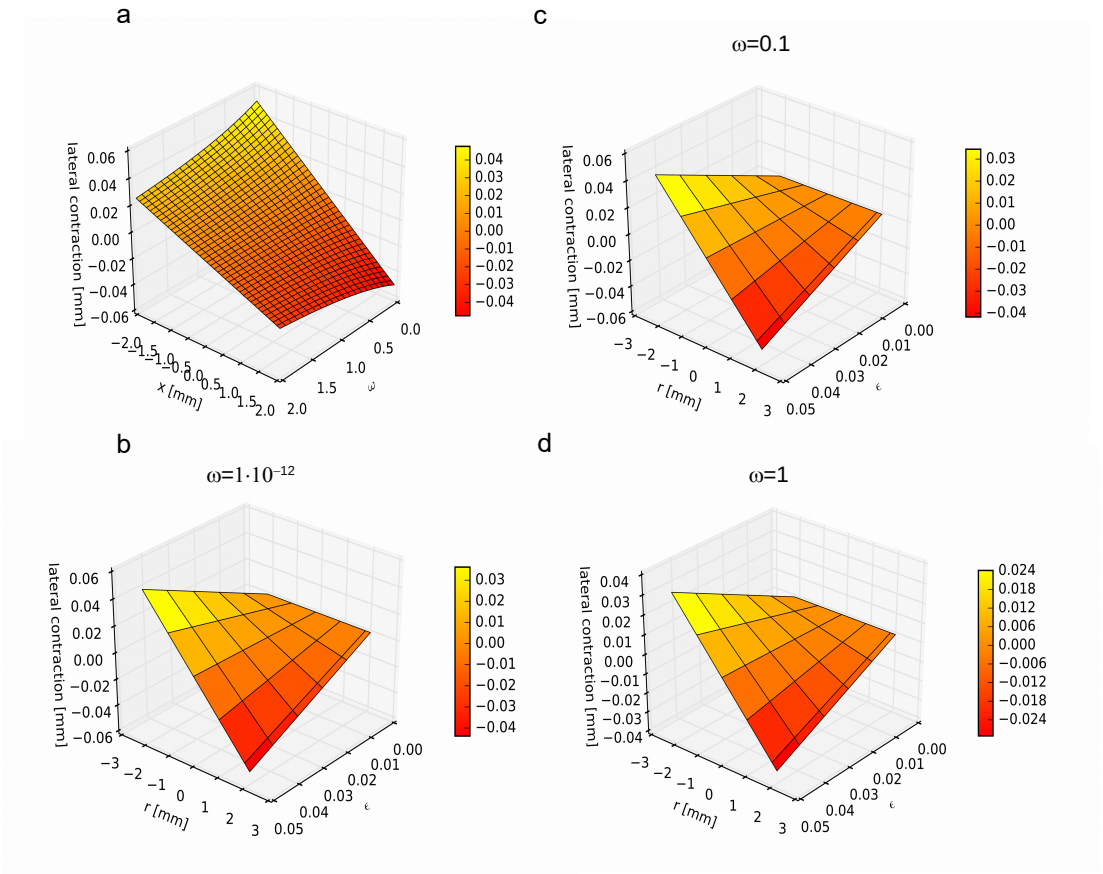

Figure 4. (**a**) Evolution of the lateral contraction with the variation of the distance from the center of nerve section for the maximum strain ($\epsilon = 0.05$) and $0 < \omega \leq 2$. (**b**) Evolution of the lateral contraction with the variation of the distance from the center of nerve section for $0 \leq \epsilon \leq 0.05$ and $\omega = 1 \times 10^{-12}$ (fully incompressible solid). (**c**) Evolution of the lateral contraction with the variation of the distance from the center of nerve section for $0 \leq \epsilon \leq 0.05$ and $\omega = 0.1$ (nearly incompressible solid). (**d**) Evolution of the lateral contraction with the variation of the distance from the center of nerve section for $0 \leq \epsilon \leq 0.05$ and $\omega = 1$ (compressible solid).

Finally, the variation of the lateral contraction as a function of the distance $r = \sqrt{(x^2 + y^2)}$ from the center of the section, and for different values of the compressibility parameter ω, was shown in Figure 5, for a longitudinal strain of 0.05. In particular, the change of the amount of lateral compression was shown by comparing a fully incompressible material (i.e., $\omega = 1 \times 10^{-12}$), a nearly incompressible material (i.e., $\omega = 0.01$), and a compressible material (i.e., $\omega = 1$).

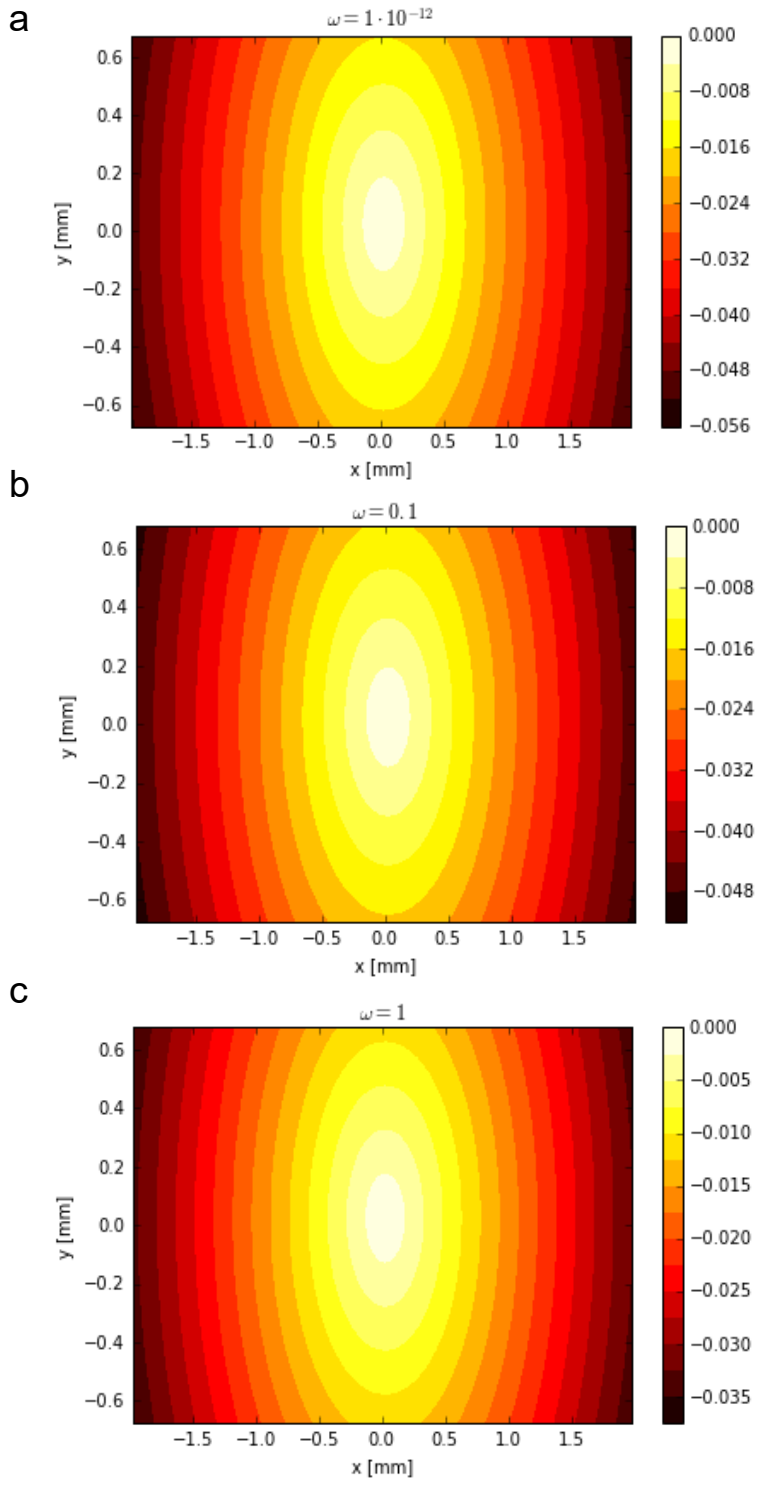

Figure 5. (**a**) Variation of the lateral contraction as a function of the distance r (from the center of the cross section) for a longitudinal strain of 0.05 and $\omega = 1 \times 10^{-12}$. (**b**) Variation of the lateral contraction as a function of the distance r (from the center of the cross section) for a longitudinal strain of 0.05 and $\omega = 0.1$. (**c**) Variation of the lateral contraction as a function of the distance r (from the center of the cross section) for a longitudinal strain of 0.05 and $\omega = 1$.

4. Discussion

The knowledge of the peripheral nerves behaviour is strategic in different scientific fields such as anatomy [29], physiotherapy [25], neuroengineering [17]. Here, the suitability of a classic approach, which was originally provided only for infinitesimal strains (i.e., $\epsilon \to 0$) [30], was proven to be valid in a physiologically relevant range of strains (i.e., $0 \leq \epsilon \leq 0.05$) [25], for which the experimental evolution of the stress was closely reproduced ($R^2 = 0.997$).

To provide a closed form theoretical solution for the proposed model, some simplifications were used. First, the nervous tissue was considered as an homogeneous and isotropic material, neglecting further anatomical details [6]. However, since the mechanical response of all the nervous substructures was expected to be similar [9], this hypothesis was acceptable. In addition, the provided relationships between strain, stress and displacements were valid for portions of nerve, which were far enough from other biological structures, which could act as further constraints to their extension. Indeed, to account for the action of the external solicitations a classic hypothesis (De Saint Venant [30]) was used. As a consequence, the action of the external system of forces and couples (which was in general unknown) was accounted for through the resultant action of all forces and moments. Therefore, the more the section of nerve was distant from border effects due to the presence of other bodies, the more the approximation given by the proposed procedure was accurate. In our case, the tensional state inside long nerves (as the sciatic one) was expected to satisfy these conditions, thus the field of displacements, coming from the theoretical tensional state, was expected to be a suitable approximation. On the contrary, for highly constrained sections of nerves in close contact to other biological structures, a more complex tensional state was expected, and a more complex displacement field was guessed.

The effects of the change of the material compressibility were also explored though the variation of the parameter (ω). First, the compressibility parameter was set to be very small (i.e., $\omega = 1 \times 10^{-12}$) and the Poisson ratio, as well as the bulk and shear modulus were computed. In particular, the presented approach was able to provide a very high value for the bulk modulus (i.e., 1.413×10^{13} kPa), while the shear modulus closely approached to a third of the Young modulus. Then, the nerve was considered respectively as a nearly incompressible solid (i.e., $\omega = 0.1$) and as a compressible one ($\omega = 1$). In these cases, the bulk modulus decreased of 9.555×10^{10} times from $\omega = 1 \times 10^{-12}$ to $\omega = 0.1$, while there was a further decrease of 7.023 times from $\omega = 0.1$ to $\omega = 1$. On the contrary, the shear modulus varied of 0.984 times between the fully and the nearly incompressible cases, while it decreased of 0.903 times from the nearly incompressible case to the compressible one. In other words, the variation of the shear modulus was extremely small in comparison to the theoretical variation of the bulk modulus.

The internal field of displacement was also explored for different degrees of compressibility of the nerve. Indeed, although the axial displacements were not affected by changes of compressibility, the displacements within the cross sectional area were influenced by the variation of the Poisson ratio. First, the provided framework was able to investigate the evolution of the displacement field for a solid with $\omega = 1 \times 10^{-12}$, that is for a material with a very high degree of incompressibility, when other computational approaches, relying on finite element modelling, may lead to not converging solutions [16]. Then, the internal fields were studied for a nearly incompressible solid (i.e., $\omega = 0.1$), as well as for a compressible material ($\omega = 1$). In all these cases, the displacement field was similar, even if they had a different amount. In other words, a smaller transversal contraction was observed for the same amount of deformation.

Although the provided model was built by using several hypothesis and simplified boundary conditions it was able to help in understanding something of the complex structure of peripheral nerves [6]. Indeed, their organization is not obvious from the perspective of the structural biology. More specifically, it is well known that sheaths of connective tissues are mainly located in the outer part of the section, while nervous bundles are mainly grouped in the inner part [7]. In addition, the nervous fibers lye inside the endoneural space, which is filled by organic liquid. As a consequence, even if protected by the external layers, the inner nervous fiber could be damaged from an increasing

pressure due to the contraction of the endoneural liquid [31]. Nevertheless, as shown in Figure 5, the lateral contraction was narrowed to the outer part of the cross section, while all the zones, which are near to the central axis (i.e., near to the barycenter of the section) were contracted only of a small extent. This consideration, could contribute on sheading light on the reason why the nervous architecture is organized "from the inner to the outer", providing the more important structures (nervous bundles) near to the center of the nerve and the reinforcing connective tissue all around the bundles. In addition, the tendency to laterally contract [9], also could explain why the different nervous bundles are spaced by connective tissue and mast cells [32]. Indeed, these materials could create a sort of protective layer, avoiding the reciprocal squeezing of bundles and preserving the internal axons from compressions. Intriguingly, even if the global anatomical structure of different peripheral nerves is apparently very similar (i.e., external layers of connective tissue and internal nervous fascicles) the position of each fascicle, with respect to other fascicles, may change inside the nerve and along its length. In other words, the internal organization of fascicles may change from proximal to distal sections of the same nerve [33], thus the distance between the central axis of the nerve and each fascicle may be variable. As a consequence, nervous fascicles seem to be affected by lateral contraction also depending on their location on the nerve trunk. In particular, recent data support the notion that centrally located fascicles contain nerve fibers targeting distal structures, while peripheral bundles leave the nerve more proximally [34]. Therefore, fascicles innervating proximal structures seem to be exposed to a greater lateral contraction within the portion of nerve running close to these structures. The presented model could be also integrated, in future studies, to other models accounting for the ability of the nervous tissue to regenerate [35–40] to better explore the connection between engineered biomaterials and the neural tissue.

Author Contributions: Conceptualization, methodology, software, validation, P.N.S.; investigation, E.G., M.R.S., A.C., P.N.S.; resources, E.G., M.R.S., P.N.S.; writing–original draft preparation, P.N.S.; writing–review and editing, E.G., M.R.S., A.C., P.N.S.; supervision, P.N.S.

Funding: This research received no external funding

Conflicts of Interest: The authors declare no conflict of interest.

References

1. Rodriguez, F.J.; Giannini, C.; Spinner, R.J.; Perry, A. 15-Tumors of Peripheral Nerve. In *Practical Surgical Neuropathology: A Diagnostic Approach*, 2nd ed.; Perry, A., Brat, D.J., Eds.; Elsevier: New York, NY, USA, 2018; pp. 323–373.
2. Scheithauer, B.W.; Kovacs, K.; Horvath, E.; Silva, A.I.; Lloyd, R.V. 18-Pathology of the Pituitary and Sellar Region. In *Practical Surgical Neuropathology*; Perry, A., Brat, D.J., Eds.; Churchill Livingstone: New York, NY, USA, 2010; pp. 371–416.
3. Nukada, H. Ischemia and diabetic neuropathy. In *Diabetes and the Nervous System*; Handbook of Clinical Neurology; Zochodne, D.W., Malik, R.A., Eds.; Elsevier: New York, NY, USA, 2014; Chapter 31, Volume 126, pp. 469–487.
4. Lundborg, G.; Hansson, H.A. Regeneration of peripheral nerve through a preformed tissue space. Preliminary observations on the reorganization of regenerating nerve fibres and perineurium. *Brain Res.* **1979**, *178*, 573–576. [CrossRef]
5. Zochodne, D.W.; Low, P.A. Adrenergic control of nerve blood flow. *Exp. Neurol.* **1990**, *109*, 300–307. [CrossRef]
6. Sunderland, S. The intraneural topography of the radial, median and ulnar nerves. *Brain* **1945**, *68*, 243–299. [CrossRef] [PubMed]
7. Sunderland, S. The connective tissues of peripheral nerves. *Brain* **1965**, *88*, 841–854. [CrossRef] [PubMed]
8. Millesi, H. The nerve gap. Theory and clinical practice. *Hand Clin.* **1986**, *2*, 651–663. [PubMed]
9. Millesi, H.; Zoch, G.; Reihsner, R. Mechanical properties of peripheral nerves. *Clin. Orthop. Relat. Res.* **1995**, *314*, 76–83. [CrossRef]
10. Zienkiewicz, O.C. *The Finite Element Method*; McGraw-Hill Company: London, UK, 1977.

11. Cook, R.D. *Concepts and Applications of Finite Element Analysis*; John Wiley and Sons: New York, NY, USA, 1981.
12. Bathe, K.J. *Finite Element Procedures*; Prentice-Hall: Englewood Cliffs, NJ, USA, 1996.
13. Main, E.K.; Goetz, J.E.; Rudert, M.J.; Goreham-Voss, C.M.; Brown, T.D. Apparent transverse compressive material properties of the digital flexor tendons and the median nerve in the carpal tunnel. *J. Biomech.* **2011**, *44*, 863–868. [CrossRef]
14. Ma, Z.; Hu, S.; Tan, J.S.; Myer, C.; Njus, N.M.; Xia, Z. In vitro and in vivo mechanical properties of human ulnar and median nerves. *J. Biomed. Mater. Res. A* **2013**, *101*, 2718–2725. [CrossRef]
15. Giannessi, E.; Stornelli, M.R.; Sergi, P.N. A unified approach to model peripheral nerves across different animal species. *PeerJ* **2017**, *5*, e4005. [CrossRef]
16. Giannessi, E.; Stornelli, M.R.; Sergi, P.N. Fast in silico assessment of physical stress for peripheral nerves. *Med. Biol. Eng. Comput.* **2018**. [CrossRef]
17. Navarro, X.; Krueger, T.B.; Lago, N.; Micera, S.; Stieglitz, T.; Dario, P. A critical review of interfaces with the peripheral nervous system for the control of neuroprostheses and hybrid bionic systems. *J. Peripher. Nerv. Syst.* **2005**, *10*, 229–258. [CrossRef] [PubMed]
18. Grill, W.M.; Norman, S.E.; Bellamkonda, R.V. Implanted neural interfaces: Biochallenges and engineered solutions. *Annu. Rev. Biomed. Eng.* **2009**, *11*, 1–24. [CrossRef]
19. Sergi, P.N.; Carrozza, M.C.; Dario, P.; Micera, S. Biomechanical characterization of needle piercing into peripheral nervous tissue. *IEEE Trans. Biomed. Eng.* **2006**, *53*, 2373–2386. [CrossRef] [PubMed]
20. Cutrone, A.; Sergi, P.N.; Bossi, S.; Micera, S. Modelization of a self-opening peripheral neural interface: A feasibility study. *Med. Eng. Phys.* **2011**, *33*, 1254–1261. [CrossRef] [PubMed]
21. Yoshida, K.; Lewinsky, I.; Nielsen, M.; Hylleberg, M. Implantation mechanics of tungsten microneedles into peripheral nerve trunks. *Med. Biol. Eng. Comput.* **2007**, *45*, 413–420. [CrossRef] [PubMed]
22. Sergi, P.N.; Jensen, W.; Micera, S.; Yoshida, K. In vivo interactions between tungsten microneedles and peripheral nerves. *Med. Eng. Phys.* **2012**, *34*, 747–755. [CrossRef] [PubMed]
23. Sergi, P.N.; Jensen, W.; Yoshida, K. Interactions among biotic and abiotic factors affect the reliability of tungsten microneedles puncturing in vitro and in vivo peripheral nerves: A hybrid computational approach. *Mater. Sci. Eng. C* **2016**, *59*, 1089–1099. [CrossRef]
24. Bhidayasiri, R.; Tarsy, D. Neuropathic Tremor. In *Movement Disorders: A Video Atlas: A Video Atlas*; Humana Press: Totowa, NJ, USA, 2012; pp. 72–73.
25. Topp, K.S.; Boyd, B.S. Structure and biomechanics of peripheral nerves: Nerve responses to physical stresses and implications for physical therapist practice. *Phys. Ther.* **2006**, *86*, 92–109. [CrossRef]
26. Capurso, M. *Lezioni di Scienza delle Costruzioni (In Italian)*; Pitagora Editrice: Bologna, Italy, 1984.
27. Bora, F.W.; Richardson, S.; Black, J. The biomechanical responses to tension in a peripheral nerve. *J. Hand Surg.* **1980**, *5*, 21–25. [CrossRef]
28. Fung, Y.C. *Biomechanics, Mechanical Properties of Living Tissues*; Springer: New York, NY, USA, 1993.
29. Sunderland, S. Anatomical features of nerve trunks in relation to nerve injury and nerve repair. *Clin. Neurosurg.* **1970**, *17*, 38–62. [CrossRef]
30. Love, A. *A Treatise on the Mathematical Theory of Elasticity*; Dover Publications: New York, NY, USA, 1927.
31. Grewal, R.; Xu, J.; Sotereanos, D.; Woo, S.L. Biomechanical properties of peripheral nerves. *Hand Clin.* **1996**, *12*, 195–204. [PubMed]
32. Sunderland, S. The adipose tissue of peripheral nerves. *Brain* **1945**, *68*, 118–122. [CrossRef] [PubMed]
33. Zhong, Y.; Wang, L.; Dong, J.; Zhang, Y.; Luo, P.; Qi, J.; Liu, X.; Xian, C.J. Three-dimensional Reconstruction of Peripheral Nerve Internal Fascicular Groups. *Sci. Rep.* **2015**, *5*, 17168. [CrossRef] [PubMed]
34. Delgado-Martnez, I.; Badia, J.; Pascual-Font, A.; Rodrguez-Baeza, A.; Navarro, X. Fascicular Topography of the Human Median Nerve for Neuroprosthetic Surgery. *Front. Neurosci.* **2016**, *10*, 286. [CrossRef] [PubMed]
35. Ciofani, G.; Sergi, P.N.; Carpaneto, J.; Micera, S. A hybrid approach for the control of axonal outgrowth: Preliminary simulation results. *Med. Biol. Eng. Comput.* **2011**, *49*, 163–170. [CrossRef] [PubMed]
36. Sergi, P.N.; Morana Roccasalvo, I.; Tonazzini, I.; Cecchini, M.; Micera, S. Cell Guidance on Nanogratings: A Computational Model of the Interplay between PC12 Growth Cones and Nanostructures. *PLoS ONE* **2013**, *8*, E70304. [CrossRef] [PubMed]
37. Spira, M.E.; Hai, A. Multi-electrode array technologies for neuroscience and cardiology. *Nat. Nanotechnol.* **2013**, *8*, 83. [CrossRef]

38. Sergi, P.N.; Marino, A.; Ciofani, G. Deterministic control of mean alignment and elongation of neuron-like cells by grating geometry: A computational approach. *Integr. Biol.* **2015**, *7*, 1242–1252. [CrossRef]
39. Roccasalvo, I.M.; Micera, S.; Sergi, P.N. A hybrid computational model to predict chemotactic guidance of growth cones. *Sci. Rep.* **2015**, *5*, 11340. [CrossRef]
40. Sergi, P.N.; Cavalcanti-Adam, E.A. Biomaterials and computation: A strategic alliance to investigate emergent responses of neural cells. *Biomater. Sci.* **2017**, *5*, 648–657. [CrossRef]